Polymer 100 (2016) 149–157

Contents lists available at ScienceDirect

Polymer

journal homepage: www.elsevier.com/locate/polymer

Glass transition of soft segments in phase-mixed poly(urethane urea) elastomers by time-domain ^{1}H and ^{13}C solid-state NMR

Weiguo Hu [a, *], Nitin V. Patil [a, 1], Alex J. Hsieh [b]

[a] University of Massachusetts, Department of Polymer Science & Engineering, Amherst, MA 01003, USA
[b] U.S. Army Research Laboratory, RDRL-WMM-G, Aberdeen Proving Ground, MD 21005-5069, USA

ARTICLE INFO

Article history:
Received 23 May 2016
Received in revised form
26 July 2016
Accepted 4 August 2016
Available online 8 August 2016

Keywords:
Poly(urethane urea)
Solid-state NMR
Glass transition

ABSTRACT

The glass transition processes of the soft-segments (SS) in a series of poly(urethane urea) (PUU) elastomers were studied by solid-state NMR. Two SS fractions, rigid (SS_r) and mobile (SS_m), can be discerned by time-domain wideline separation, $^{13}C-^{1}H$ dipolar dephasing, and frequency-switched Lee-Goldberg spin-locked $T_{1\rho}$ relaxation experiments. At increasing temperature, part of the SS_r population turns into SS_m, while the decay constants of both fractions only see moderate changes. The extent of the population exchange is greater for samples with more phase mixing. This population exchange can be interpreted as the glass transition in the SS-rich domains. Comparison between $T_{1\rho}$ relaxations on the xy plane and along the magic angle indicates that the domain sizes of SS_r and SS_m are likely less than 2–3 nm. SS_r is not completely rigid, but possesses both a fast, anisotropic chain rotation associated with the β relaxation and a slower motion with more isotropic nature at ca. 10^5 s^{-1}. It is predicted that at high strain rates, most of SS_r and part of SS_m would become rigid, resulting in dynamically induced strengthening and toughening.

1. Introduction

Segmented polyurethanes, polyureas (PU) and poly(urethane urea)s (PUUs) are polymerization products of low-glass-transition-temperature (T_g) soft segments (SS) and high T_g, and often highly polar, hard segments (HS). These elastomers have complex morphology due to the statistical distribution of the thermodynamically incompatible hard and soft segments. The versatile chemistry of this class of elastomers has led to a wide range of applications in the areas of coating, adhesives, foams, and composite structures [1]. Particularly, these elastomers have the potential of transitioning from the rubbery-like into leathery-like or glassy regime with increasing strain rate, where stress levels may be greatly enhanced and large energy dissipation realized [2,3]. This was highlighted by Roland and co-workers in their proposed deformation induced glass transition mechanism [2] as a plausible pathway towards effective impact energy absorption or dissipation, in contrast to other potential mechanisms such as strain delocalization, shock impedance mismatch, and shock wave dispersion [4].

In PUUs, reaction of diisocyanates with diols and diamines results in urethane and urea moieties, respectively. The latter can self-assemble via intermolecular hydrogen bonding to form hard segment domains. On the other hand, various degrees of phase mixing between hard and soft segments exist due to statistical sequence distribution and intermolecular interactions [5]. This causes the shift in T_g of HS compared to that of its respective component in the pure bulk state, which could be used to assess the extent of phase mixing with suitably constructed thermodynamic models and certain assumptions [6]. Characterization techniques such as differential scanning calorimetry (DSC) [6–8], dynamic mechanical analysis (DMA) [3,7], small-angle X-ray scattering (SAXS) [6,8–11], atomic force microscopy (AFM) [11,12], broadband dielectric spectroscopy (DES) [13], Fourier-transformation infrared (FTIR) [7,10,11], and solid-state nuclear magnetic resonance (ssNMR) spectroscopy [9,14–17] have been used to analyze the phase mixing behavior of polyurethanes, polyureas, and PUUs.

Recently, PUU elastomers consisting of soft segments of small molecular weights have exhibited greater phase mixing as indicated by a drastic shift and a substantial broadening of the glass transition process of SS, which strongly influenced the material's physical and mechanical properties [3]. The significant broadening of the glass transition process makes it difficult to apply

* Corresponding author.
E-mail address: whu@data.pse.umass.edu (W. Hu).
[1] Current address: Reichhold Inc., 1035 Swabia Court, Durham, NC 27703, USA.

http://dx.doi.org/10.1016/j.polymer.2016.08.015
0032-3861/

thermodynamic models [6] simply based on the shift of T_g to gain detailed insight of phase mixing. Generally, compared to the extensively studied glass transitions in homogeneous amorphous polymers, glass transitions in heterogeneous polymers as measured by DSC [18] and dielectric experiments [19] are much broader. Factors such as the correlation length of the transition being long compared to the transitioning domains [19] and the broad distribution of domain sizes and geometries could contribute to the broadening.

A number of ssNMR studies have been dedicated to the morphological and dynamical behavior of polyurethanes [9,14,15,20,21]. In particular, the dynamics of the hard segments and at the HS/SS interfaces has received the majority of the attention [9,14,15,17]. On the other hand, the detailed dynamical behavior in the SS-rich domains has not been extensively studied. Using ^{13}C T_1 relaxation measurements, Ishida et al. [14] found that the SS in a polyurethane to be mostly of a single dynamical component except for a small (ca. 4% of SS) interfacial fraction. While ^{13}C T_1 relaxation is sensitive to fast molecular dynamics at the 10^8 s^{-1} window, in a recent work [22], we used NMR techniques that were more sensitive to slower dynamics (10^5 s^{-1}), and identified two major dynamical fractions in SS-rich domains. In the present report, we will use a number of experiments to confirm that these two fractions are related via glass transition.

ssNMR is potentially able to provide a unique perspective to the broad glass transitions in that it could stay at a given temperature indefinitely and measure the participating populations and their dynamical states at this temperature. This is unlike DSC, DMA, or DES, which must continuously scan through the entire temperature (or test frequency) window. By taking successive NMR measurements at each temperature step, the broad transition can then be dissected to slices or subpopulations, with each slice having its own T_g. This would provide a unique and in-depth understanding of the transition mechanisms. The challenge of using ssNMR to study the glass transition in PUU lies in the difficulty of separating the glassy and rubbery components because their NMR peaks often overlap as both components often have similar conformations. In this report, we use several techniques to probe this problem. First, we use ^1H time domain signal, which can distinguish rubbery component from rigid component, but lacks chemical resolution and thus cannot separate HS transitions from SS transitions. Next we use wideline separation (WISE) NMR technique, which is able to separate the rigid- and mobile-SS fractions and reveal their relationship via glass transition. As WISE is not a quantitative technique, we next conduct ^{13}C direct-polarized ^1H–^{13}C dipolar dephasing experiments, which confirm the WISE observations and supply quantitative information about the participants of the glass transition. Then, by studying $T_{1\rho}$ relaxations with and without the influence of spin diffusion, the segmental motion rates for the two dynamical SS components and their domain sizes are assessed. Finally, ^{13}C spin-lattice relaxation is utilized to understand the fast, local segmental dynamics in the SS domains. Following the time-temperature superposition principle, we attempt to exploit the ssNMR data to infer the trend in the dynamic response of PUUs under high-strain-rate deformation.

2. Experimental section

2.1. Materials

PUU elastomers consisting of 4,4'-dicyclohexylmethylene diisocyanate (HMDI), diethyltoluenediamine (DETA), and poly(tetramethylene oxide) (PTMO) were prepared using a two-step prepolymer synthesis method [3]. The molecular weights (MW) of PTMO were 650, 1000, and 2000 g/mol. All PUU samples were named using two sets of numbers designating the molar ratios of HMDI:DETA:PTMO and the molecular weights of PTMO in g/mol, respectively. For example, sample 211–2k has ingredient molar ratio HMDI:DETA:PTMO = 2:1:1, with PTMO MW of 2000 g/mol. Four PUU samples were studied: 211–650, 211-1k, 211-2k, and 321-2k. The samples with longer SS, 211-2k and 321-2k, are more phase-separated and have less extent of phase mixing, while samples 211-1k and 211–650 exhibit greater phase mixing. Following the conventions for polyurethane and poly(urethane urea) family of polymers, the terminology of hard and soft segments in this report strictly refers to the chemical identities of the building blocks in PUUs, with HMDI and DETA as HS, and PTMO as SS. The prefixes rigid- and mobile-will be used to describe physical behaviors. Note that chemically designated SS can be physically either mobile or rigid. So does chemically designated HS.

2.2. NMR measurements

The following experiments were conducted on a Bruker Avance III 600 MHz standard-bore spectrometer, operating at a ^1H frequency of 600.14 MHz and ^{13}C frequency of 150.90 MHz, in a 4 mm CP/MAS probe: (1) ^1H FIDs were collected using a solid echo sequence, at non-spinning condition, with pre- and post-echo delays of 4.6 μs and 0 μs, respectively. 90° pulse length, dwell time, and dead time were 2.5 μs, 0.4 μs, and 4.6 μs, respectively. To fit the real part of the wideline signal, the receiver phase was adjusted such that the imaginary part of the signal was minimized. The carrier frequency was set on resonance before all the experiments. Probe background ^1H signal was collected by acquiring signal from an empty rotor and subsequently subtracted from all the FIDs before fitting. The differences in signal intensity between the solid echo and the single-90 FID for both the rigid and the mobile components were ca. 2% (see Supplemental Materials for more details). These differences are smaller than what had been reported in the literature [23] projected to a delay of 4.6 μs, which suggests that the dependence of the differences between the solid echo and the single pulse FID on the delay time may not be linear. (2) ^{13}C direct-polarized ^1H–^{13}C dipolar dephasing experiments. The pulse sequence is a ^{13}C 90° pulse followed by a variable free evolution (dephasing under ^1H–^{13}C dipolar coupling) period and ^1H high-power decoupling during detection. Instead of using a 180° pulse in the middle of the dephasing period to refocus chemical shift evolution, the PTMO ether carbon signal at 71 ppm was put on resonance so that the decay at 0–10 μs can be accurately recorded and there was no evolution due to chemical shift for this peak. (3) $T_{1\rho}$ relaxation experiments of sample 211-1k and 321-2k. Relaxations under spin lock (SL) on xy plane, under simple Lee-Goldberg (LG) scheme, and under frequency-switched Lee-Goldberg (FSLG) sequence were studied. Contact time was 0.6, 0.8, and 1 ms at ≤ 300 K, 322 K, and 334 K, respectively, in order to obtain a balance between optimal signal sensitivity and minimal spin diffusion. All the SL periods were applied before CP. During SL, the regular LG pulse was applied for LG-SL, and FSLG pulses were applied for FSLG-SL. During CP, the regular LG pulse was used on the ^1H channel for both LG-SL and FSLG-SL. Spin lock fields were 64.1, 78.5, and 78.5 kHz for xy-SL, LG-SL, and FSLG-SL, respectively. Samples were packed in the middle 1/3 of rotor in order to minimize B_1 field inhomogeneity.

The following NMR experiments were performed on a Bruker DSX300 wide-bore spectrometer, operating at a ^1H frequency of 300.12 MHz and ^{13}C frequency of 75.47 MHz, in a 4 mm CP/MAS probe. (1) WIdeline SEparation (WISE) experiments starts with π/2 excitation pulse followed by an evolution period (t_1) and then transfer of magnetization from proton to carbon using ramped cross-polarization (CP) and proton-decoupled ^{13}C detection [24].

Dwell time of 8 μs was used for PUU samples. Contact time of 1 ms (except for 211-2k, for which 1.6 ms was used due to the high mobility of its SS-rich domains), ramp size of 5 kHz, magic-angle spinning speed of 5 kHz, and 160 t_1 increments were employed. (2) ^{13}C T_1 of internal methylene carbons of soft segments was determined using the Torchia method [25].

2.3. Dynamic mechanical analysis (DMA)

The DMA measurements were performed on a TA Instruments Q800 Dynamic Mechanical Analyzer. PUU samples of thickness ~1 mm were tested in an oscillatory tensile mode at a heating rate of 1 K/min and a frequency of 1 Hz, over the temperature range of 125 K–400 K.

3. Results

3.1. Time-domain ^1H NMR data

Time-domain ^1H experiment is a simple, fast, and robust technique that has been widely adopted for the study of phase structure in heterogeneous polymers. In semicrystalline polymers such as polyethylene (PE) and isotactic polypropylene (iPP), the time domain signal can usually be modeled by three components, representing the crystalline, intermediate, and amorphous phases [26,27]. The crystalline phases are often modeled by a Gaussian or Abragamian decay while both intermediate and amorphous phases usually by exponential decays. The general principle of the fitting is that it should faithfully reproduce the major features of the FID with the fewest adjustable parameters possible. Unlike PE or iPP, which typically need three components for a high-quality fit, the FIDs of polyurethanes were found to be well fitted using two components (Gaussian/exponential or bi-exponential) [20]. This was found to be true for the PUUs in the current study as well, in which we used a fast-decaying Gaussian and a slow-decaying single-exponential function to fit all the ^1H time-domain signals. Fig. 1 shows the wideline FIDs of 211-1k at 279 K and 310 K, as well as their fits. The fast-decaying component is attributed to domains with low segmental mobility (stronger ^1H–^1H dipolar coupling), whereas the slow-decaying component from domains with higher segmental mobility (weaker ^1H–^1H dipolar coupling). Good fitting quality is seen from the Figure, as the curves (fits) mostly pass through the dots (experimental data). A more complete list of the fitting results, including the fast- and slow-decaying fractions, their respective decay constants (T_{dd}, with the subscript 'dd' stands for dipolar dephasing, as the decay is primarily due to dephasing under the influence of ^1H–^1H dipolar coupling), and standard-deviations of fitting, are displayed Table S1 in Supplementary Materials. For comparison, the fractions of chemically-designated HS protons (i.e., the protons that belong to HMDI and DETA) among all protons, %HS ^1H, are calculated from the polymer compositions and shown in the table.

In Fig. 1, the fitting quality for the 279 K data is less than ideal between 20 and 40 μs. This is likely due to the existence of the HS-SS interphase component, which has a mobility that is between the two major fitting components. Similar deviations have been observed before and could be reduced by adding an intermediate component [28]. However, for PUU, the fitting quality achievable with a two-component model is still very good, e.g. much better than that for semicrystalline polymers such as polyethylene, so we choose to work with a two-component model. In fact, considering the highly complex morphology of PUU, it is remarkable that a model with only two components and three free-adjustable parameters is able to capture most of the major features of the ^1H signal.

The decay constants T_{dd} of the slow component for all the samples are at 35–160 μs (corresponding to frequency-domain full-width-at-half-maximum of ca. 2–8 kHz). Such values are typical of domains above T_g, so the slow-decaying component can be assigned to the segments that are in rubbery state, which could include SS in SS-rich domains (mobile-SS) and small amount of HS that is dissolved in them (mobile-HS). The decay constants for the fast components (12–16 μs) are typical of segments with very limited mobility, which may include phase-separated HS (rigid-HS) and those SS-rich domains that are extensively phase-mixed with HS and thus has a higher T_g (rigid-SS).

The fractions of rigid components as a function of temperature are shown in Fig. 2. It is observed that for the two samples with higher SS MW, 321-2k and 211-2k, the temperature dependence of the rigid fractions are relatively flat, decreasing by 8–10% from

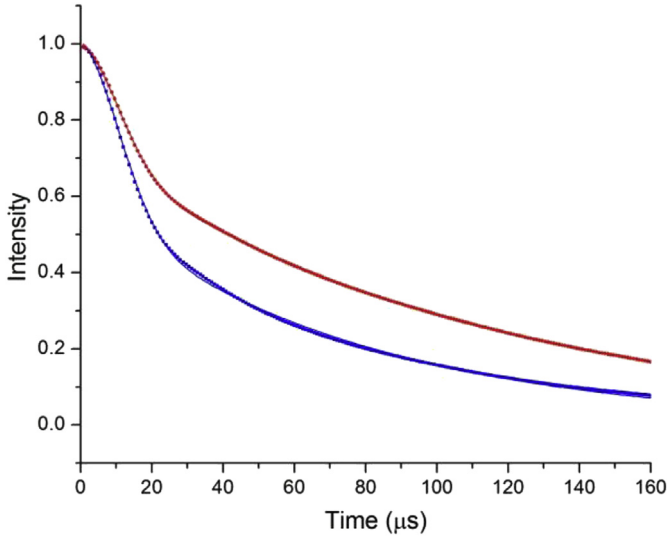

Fig. 1. ^1H FIDs (dots) of 211-1k at 279 K (blue) and 310 K (red) with their respective Gaussian-exponential fits (solid lines). (For interpretation of the references to colour in this figure legend, the reader is referred to the web version of this article.)

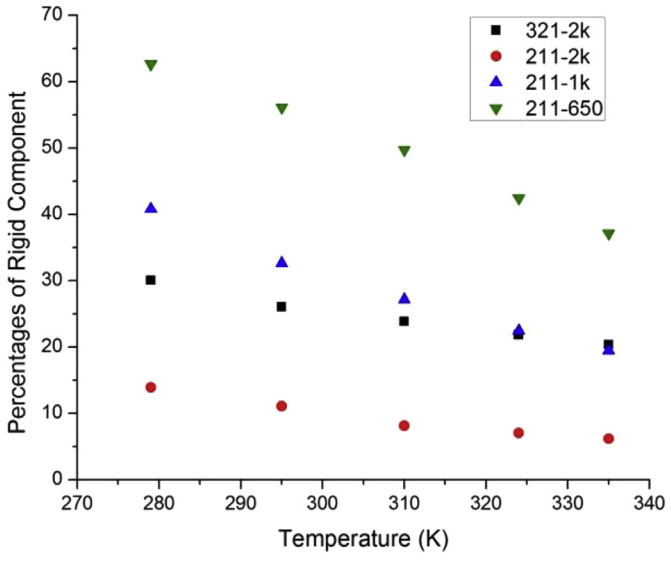

Fig. 2. Percentages of ^1H FID rigid fraction with respect to temperature for samples 321-2k (squares), 211-2k (circles), 211-1k (up triangles), and 211–650 (down triangles).

279 K to 335 K. On the other hand, the rigid fraction for samples with smaller SS MW show much steeper temperature dependence, decreasing by 21% and 26% across the same temperature window for 211-1k and 211–650, respectively.

Due to the lack of chemical resolution of the ^{1}H signals, the temperature dependence of the rigid fractions might come from the change in either rigid-HS or rigid-SS. To assess the relative contribution from them, we could compare samples 211-2k, 211-1k, and 211–650, which have exactly the same sequence distributions of HS monomers and thus the same distribution of HS-rich domain sizes. We could thus reasonably assume that their rigid-HS population would have the same temperature dependence. Therefore, the different temperature dependence of the total rigid fraction for the three samples should be mainly due to the difference in rigid-SS as a result of the different SS MW.

At increasing temperature, the T_{dd}'s of the rigid component remain mostly constant, while those of the mobile component moderately rise. But the most salient change across this window is the change of the rigid/mobile relative population. At all temperatures, all the FIDs can only be reliably fitted with two-component Gaussian-exponential decays without introducing any third component. Therefore, as temperature varies, the change occurring in these materials can be described by an exchange of population between the rigid and mobile components. The extent of this population exchange is greater for more phase-mixed samples. The mechanism of this population exchange will be further analyzed in the next section.

3.2. SS dynamic populations by high-resolution NMR

Although ^{1}H data suggest that the steep change of the rigid and mobile fractions with temperature for highly phase-mixed PUUs likely originates from the SS-rich domains, ^{1}H data do not provide chemical resolution to separate the change occurring for SS vs HS. To further probe the nature of the changes of SS dynamics in PUU, we explored two high-resolution techniques. The first is WIdeline SEparation (WISE) experiments, through ^{1}H-to-^{13}C polarization transfer and ^{13}C detection, to selectively study the dynamics of SS [24]. When the first dimension (t_1) data are processed and analyzed in the time domain using well-studied decay shapes (TD-WISE), information about the rigid and mobile fractions and decay constant of each SS component can be obtained, without complications from the changes in HS populations [22]. The decay in the first dimension (t_1) is similar to ^{1}H wideline FID except that the former is under magic angle spinning condition.

The main deficit of the WISE technique is that the CP process is inherently not quantitative. In ^{1}H time-domain NMR data, the T_{dd} of the rigid and mobile components differ by a factor of up to 10, which means that the signal rise time constants during CP, T_{CH}, could be quite different between various components of the sample. Since the ^{1}H $T_{1\rho}$ of each dynamical fractions for the polymers under study is in the order of 1.5–3 ms [22], the rigid component could be overrepresented in the spectra. In addition, spin diffusion during CP could mix rigid and mobile fractions, though this effect is likely small (see Discussions for more details on spin diffusion).

^{13}C CP/MAS spectra of HMDI/DETA/PTMO-based PUU has two tall and sharp peaks at 27 ppm and 71 ppm, from the PTMO moiety, along with other broader and shorter peaks from the HMDI and DETA moieties [22]. Fig. 3 shows the 1st dimension TD-WISE decay data for the 27 ppm peak (aliphatic CH_2 of PTMO) for sample 211-1k at select temperatures. As each data point is the integration of the 27 ppm peak, the data contains no contribution from the HS. It can be seen that the FIDs contain two components with drastically different decay rates. Therefore, two-component exponential fits were performed on the 1st dimension ^{1}H decays obtained at

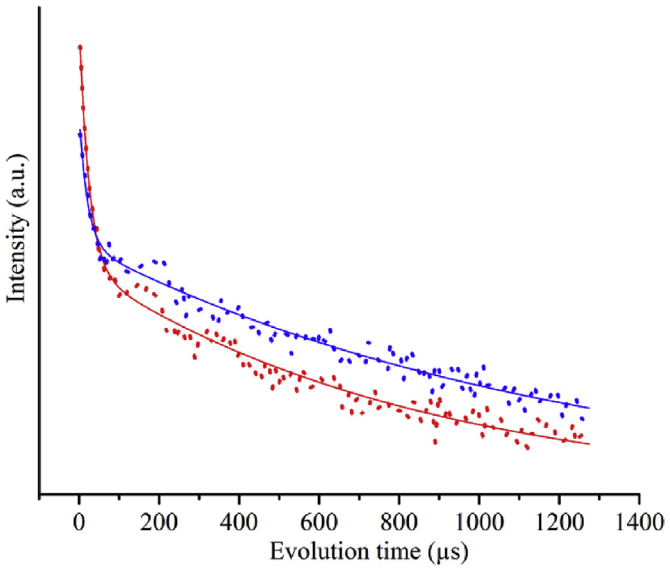

Fig. 3. First dimension ^{1}H (t_1) decay (dots) of soft segments with respect to evolution time for 211-1k at temperatures 295 K (red) and 334 K (blue) and their respective fits (lines). (For interpretation of the references to colour in this figure legend, the reader is referred to the web version of this article.)

different temperatures of PUU samples, and the results obtained are shown in Table S2 of Supplemental Information. The fits are generally of reliable quality, with the deviation mostly from random noise. The two SS populations are termed $SS_{r,W}$ (fast-decaying component) and $SS_{m,W}$ (slow-decaying component), respectively. The subscripts *r* and *m* stands for rigid and mobile, respectively, and *W* indicates that the components are obtained by WISE experiments. Two small deviations from the above general fitting procedures (for samples 321-2k and 211–650) are noted in the Supporting Information. The fitting results show that $SS_{r,W}$ population quickly decreases with increasing temperature for 211-1k and 211–650, while stays mostly unchanged for 211-2k and 321-2k. This confirms the ^{1}H FID observation that the steeper temperature dependence of the population exchange for the more phase-mixed samples is due to the change in SS.

To address the non-quantitative aspect of the TD-WISE method, we take advantage of the short SS ^{13}C T_1 relaxation times (see ^{13}C T_1 Relaxation section below), and use ^{13}C direct polarization (DP) followed by a free evolution, during which the decay as a result of ^{1}H–^{13}C dipolar coupling can be monitored. The segments that have short ^{1}H–^{1}H dephasing time due to low mobility would also have short ^{1}H–^{13}C dephasing time, while mobile segments would have both long ^{1}H–^{1}H and long ^{1}H–^{13}C dephasing times. Therefore, this method would give similar information as the TD-WISE method, except without the uncertainty introduced by cross polarization. The ^{1}H–^{13}C dipolar dephasing method has been widely used to distinguish chemical structures [17,29] (e.g. protonated vs. non-protonated), motional geometries [29,30] (e.g. uniaxial vs. isotropic tumbling), and domains [31] (e.g. glassy vs. rubbery) with different ^{1}H–^{13}C coupling strengths. The fast-decaying component was found to usually follow Gaussian behavior, while the slow-decaying component often an exponential one [29]. In polyurethanes, it has been reported that the ^{1}H–^{13}C dipolar dephasing behavior of HS signal has a fast- and a slow-decaying component, which could be attributed to phase-separated and phase-mixed domains, respectively [17].

The effect of MAS to the ^{1}H–^{13}C dephasing decays here needs to be considered. The decay of the rigid-SS is under the influence of

strong (>20 kHz) $^{1}H-^{13}C$ couplings and $^{1}H-^{1}H$ couplings, thus would decay very quickly within the first 40–50 μs following Gaussian decaying behavior [29]. Thereafter, modulation by MAS and $^{1}H-^{13}C$ couplings generates rather complex dependence of signal intensity as a function of evolution time, then a small rotational echo at one full rotor period, due to partial refocusing of the dipolar coupling [29]. The rotational echoes at subsequent integer rotor periods are still smaller. On the other hand, the mobile-SS has much attenuated dipolar couplings and follows a slow exponential decaying behavior under MAS [29]. Therefore, we sampled the decays at short intervals at 0–40 μs, to capture the rigid-SS component, and at multiples of rotor period at 200–1200 μs, to capture the mobile-SS component. The area of the on-resonance ether carbon peak at 71 ppm was plotted.

An alternative way to the on-resonance free evolution is a rotor-synchronized Hahn-Echo experiment. We conducted this experiment for sample 211-1k and found that it gave very similar results for rigid and mobile fractions as the free evolution experiment. It gave slightly longer decay constant for the mobile fraction, likely because the Hahn Echo refocused some additional chemical shift anisotropy, while the free evolution does not. To probe the possible shift of rotation echo peak position, we added sampling points to our free evolution experiment to include data points within ±50 μs of the rotational echo. No detectable shifts of the echo peaks position were found.

The ^{13}C dephasing signals can be well fitted by two-component decays, with the fast-decaying component modeled as Gaussian and the slow-decaying component as exponential. The signals and their fits for 211–650 at 279 K and 335 K are shown in Fig. 4. The data points at first rotor period (200 μs) do not notably deviate from the exponential curve, suggesting that the first rotational echo generated by the rigid-SS component is negligible. Therefore, the amplitudes of the Gaussian and exponential components should reasonably reflect the populations of the rigid- and mobile-SS (termed $SS_{r,D}$ and $SS_{m,D}$, in which D stands for $^{1}H-^{13}C$ dipolar coupling) respectively.

Fig. 5 shows the $SS_{r,D}$ population for all the samples as a function of temperature ($SS_{r,D} + SS_{m,D} = 100\%$). When the $SS_{r,D}$ population is less than a few percent, which is the case for 321-2k at T > 300 K, for 211-2k at T > 290 K, and for 211-1k at T > 330 K, the fitting results become less reliable and thus are not plotted. Fig. 5 shows that the rigid-SS population decreases and mobile-SS increases for samples 211-1k and 211–650 at increasing temperatures. For the samples with higher SS MW, 211-2k and 321-2k, the rigid-SS population is only 3%–4% at the lowest temperatures, and become negligible at higher temperatures. These observations are qualitatively consistent with the findings in TD-WISE experiments, though quantitatively the populations obtained by the fitting are quite different. For each sample, $SS_{r,D}$ is much smaller than $SS_{r,W}$, and the differences are larger for the cases where the decay constants of the mobile-SS components are higher (which means lower CP efficiency). This should mainly be because TD-WISE involves CP, which over-represents the rigid population. The more detailed $^{13}C-^{1}H$ dipolar dephasing fitting results are shown in Table S3 in Supplemental Information.

To interpret these observations, we compare with the data from

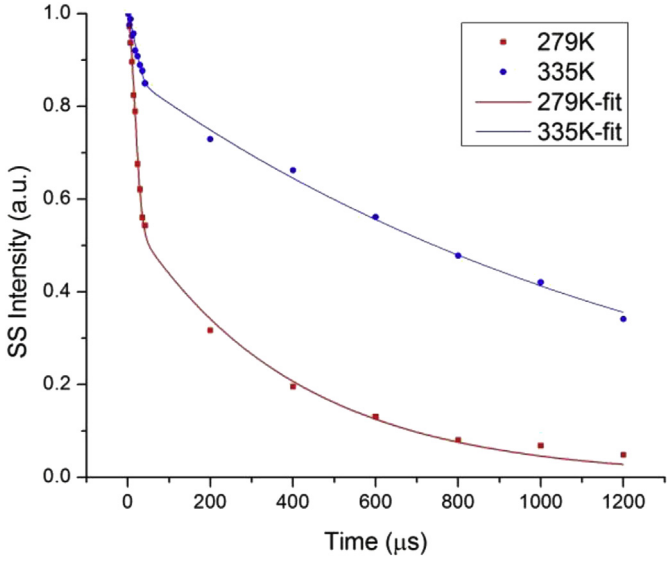

Fig. 4. $^{13}C-^{1}H$ dephasing decay (dots) of soft segments with respect to evolution time for 211–650 at temperatures 279 K (red) and 335 K (blue) and their respective fits (lines). (For interpretation of the references to colour in this figure legend, the reader is referred to the web version of this article.)

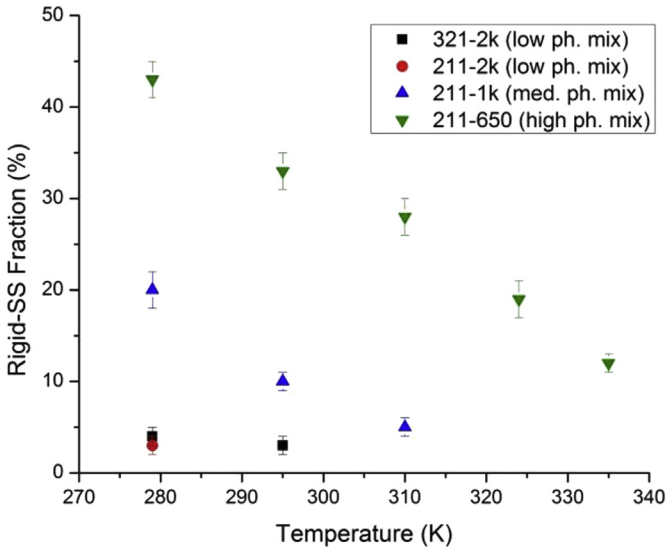

Fig. 5. $SS_{r,D}$ fraction (%) in $^{13}C-^{1}H$ dipolar dephasing experiments for samples 321-2k (squares), 211-2k (circles), 211-1k (up triangles), and 211–650 (down triangles).

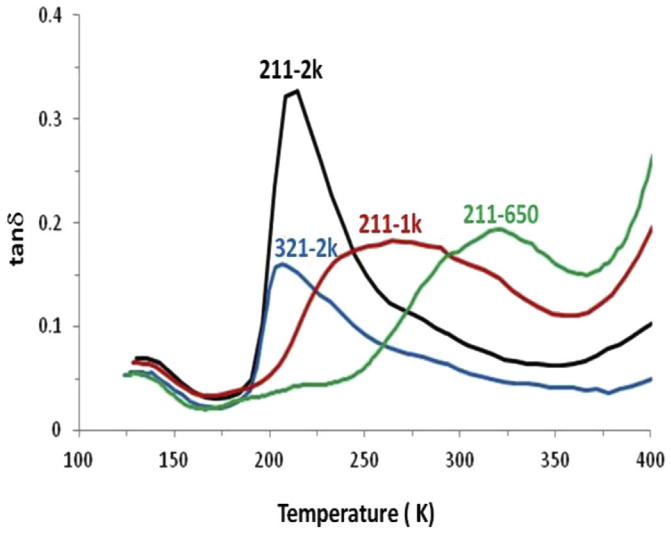

Fig. 6. DMA tanδ vs temperature for 211-2k (black), 321-2k (blue), 211-1k (red), and 211–650 (green). (For interpretation of the references to colour in this figure legend, the reader is referred to the web version of this article.)

DMA measurements. In the DMA tanδ curves shown in Fig. 6 (part of the results, DMA data for 211-2k, 211-1k, and 211-650, has been reported in Ref. [12]), substantial differences between the SS glass transitions in these PUUs can be observed. For both 321-2k and 211-2k, there is a distinct relaxation peak at 200–210 K along with a weak high-temperature-side shoulder. This strong relaxation peak occurs at similar temperature and with width similar to the glass transition of bulk PTMO (DMA tanδ curve on Fig. 14.17 of ref. [32]), and can be assigned to the glass transition in phase separated SS-rich domains. The weak shoulder on the high-temperature side may be associated with the sparsely populated phase-mixed regions. The relaxation peak of 321-2k is less intense than 211-2k, which should be due to the smaller SS content of the former. The DMA curves of samples 211-1k and 211–650 exhibit substantial difference from those of 211-2k and 321-2k. Both 211-1k and 211–650 show very broad T_g, with a relaxation peak temperature at ca. 270 K and 320 K, respectively. The substantial shift in T_g with respect to that of pure PTMO suggests extensive and broad distribution of phase mixing. The DSC results of samples 211-1k and 321-2 K have been also reported in a previous publication [3] and showed similar trends as DMA, though with less details.

The criterion of defining mobile vs. rigid in TD-WISE and $^{13}C-^{1}H$ dipolar dephasing experiments is at a much higher rate than that in DMA: the former being at ca. 10^5 s^{-1}, while the latter at 1 s^{-1}. Therefore, the transitions observed by NMR would occur at higher temperatures, likely 30–40 K higher, than the same transitions observed by DMA. Similarly, shift of 50–60 K between the rigid-mobile transitions as observed by ^{2}H NMR (10^6 s^{-1}) and DSC (10^{-1} s^{-1}) have been reported [15]. With this shift in mind, we can compare the NMR data with DMA results, and it becomes clear that the transition or population exchange between the rigid and mobile fractions in NMR corresponds to the glass transition as detected in DMA. For the more phase-separated samples 321-2k and 211-2k, the rigid-SS fraction is quite small between 279 K and 335 K (corresponding to DMA test temperatures of between ca. 310 K and 370 K), which corroborates with the DMA observation that its SS glass transition is mostly complete at 300 K. For 211-1k and 211–650, the continuous transition between the rigid and mobile fractions observed by NMR at increasing temperature corresponds to the very broad glass transitions in DMA. The broad distribution of T_g for the SS population is a result of the broad distribution of phase mixing. At any given temperature, the SS population is composed of glassy and rubbery fractions, which is the reason its TD-WISE and $^{13}C-^{1}H$ dipolar-dephasing decays can be modeled by two-component decays. TD-WISE and $^{13}C-^{1}H$ dipolar-dephasing data are also consistent with ^{1}H wideline observations, both showing that the extent of population exchange dramatically increases with decreasing SS MW.

$T_{dd,mas}$ of the $SS_{m,W}$ fraction in 321-2k and 211-2k, despite the large difference in HS%, are strikingly similar; both are notably longer than those of 211-1k and 211–650. Such is also the case for $T_{dd,CH}$, the decay constants in $^{13}C-^{1}H$ dipolar-dephasing experiments. This is related to the much lower T_g of the former two samples as shown in the DMA data, and is due to the larger degree of phase separation in 321-2k and 211-2k. The ratios of decaying constants for rigid vs. mobile components in ^{1}H wideline and in TD-WISE experiments are ca. 1:4 and 1:20, respectively. This difference should be due to the effect of the moderate-speed MAS, which dramatically extends the decaying time for signals with sufficiently high mobility, while leave those with lower mobility unchanged.

3.3. $T_{1\rho}$ relaxations

Estimating from the ^{1}H and TD-WISE data, the average segmental motional rate in the SS-rich domains is likely in the neighborhood of 10^4–10^6 s^{-1}. ^{1}H $T_{1\rho}$ relaxation would be a suitable tool to further understand the dynamics at this rate range. Since $T_{1\rho}$ relaxation on the xy plane is affected by ^{1}H spin diffusion, study of relaxations with suppressed spin diffusion would also be desired. T_{1xz} relaxation [33], the relaxation along an effective field generated by a multiple-pulse homonuclear decoupling sequence (usually MREV-8 [34,35]), has been shown to be an effective probe of mid-kHz dynamics with minimal spin diffusion [36]. However, the interference between the MREV-8 sequence and magic angle spinning could lead to anomalous relaxation results [37]. In this report we study relaxations under two homonuclear-decoupled spin-lock sequences, the Lee-Goldberg (LG) sequence, and its improved version, frequency-switched Lee-Goldberg (FSLG) sequence, which are both windowless and thus could achieve cycle times (ca. 10 μs) that are much shorter than the rotor period. The Lee-Goldberg [38] (LG) sequence uses an off-resonance ^{1}H spin lock pulse so that the effective spin lock field is along the magic angle direction, which substantially suppresses $^{1}H-^{1}H$ dipolar coupling. It has been reported that spin diffusion coefficient under LG spin lock is dramatically slowed down, to ca. 1/20 of that during z-spin diffusion [39]. The frequency-switched Lee-Goldberg (FSLG) sequence [40], during which the sign of the off-resonance frequency and its phase alternate every 2π revolution around the magic angle, is an even more effective way of ^{1}H homonuclear decoupling and thus spin diffusion inhibition. Comparative study of ^{1}H relaxations along these spin lock pulses would be informative about the state of dynamics in the SS-rich domains.

Fig. 7 shows the signal area of the PTMO ether carbon peak (71 ppm) at 334 K as a function of spin lock periods for the three sequences obtained for 211-1k. The 71 ppm peak was chosen to represent the PTMO because it has no other major peaks in the immediate neighborhood so that the phase distortions from the off-resonance peaks would have a minimal impact on the integration results. On the semi-log plot, signal with spin lock on the xy plane (xy-SL) decays in a mostly linear way, with a slight bend upward at longer spin lock time, indicative of a mostly single exponential decaying behavior. On the other hand, the decays under LG-SL and FSLG-SL last longer and significantly deviate from linear. There have been few reports in the literature comparing relaxation behaviors under these pulses. For small molecules, it has been reported that relaxations under LG-SL is slower than xy-SL,

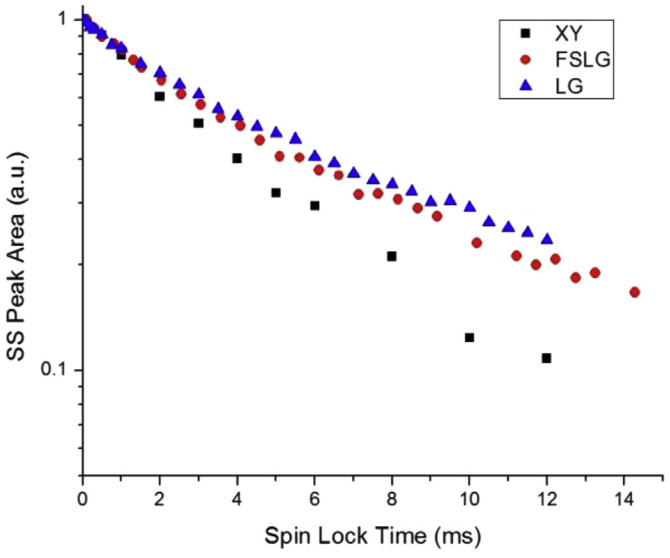

Fig. 7. $T_{1\rho}$ decay of 211-1k at 334 K under xy, LG, and FSLG spin lock conditions.

and both decays are single-exponential [41,42]. The somewhat faster decay under FSLG-SL than that under LG-SL has been observed before and attributed to the transient effect during the frequency/phase switch [42].

Since $T_{1\rho}^{LG}$ and $T_{1\rho}^{FSLG}$ are much less affected by spin diffusion than $T_{1\rho}$, the fact that $T_{1\rho}$ is nearly single exponential while $T_{1\rho}^{LG}$ and $T_{1\rho}^{FSLG}$ are pronouncedly non-exponential suggests that the non-exponential decaying nature of the latter is not due to any intrinsic nature of the dynamics, but due to a heterogeneous spatial distribution of the dynamics. As LG-SL and FSLG-SL generate similar relaxation behaviors, only FSLG-SL relaxation data are discussed in the following. The relaxations can be well-fitted by two-component exponential decay. The results are shown in Table 1.

Since the $T_{1\rho}^{FSLG}$ of both components for both samples increase with temperature, the average motional rates of both components are in the fast-motion regime relative to the spin lock field strength (78.5 kHz in this report). Judging from the shallow temperature dependences, the fast-decaying component in both samples at 280 K is quite close to the $T_{1\rho}$ minimum, and has lower mobility than the slow-decaying counterpart at all temperatures probed. Therefore, the fast- and slow-decaying components are termed $SS_{r,T}$ and $SS_{m,T}$, respectively, in the following. The subscripts *r* and *m* stands for rigid and mobile, respectively, and *T* indicates that the components are obtained by $T_{1\rho}^{FSLG}$ experiments. It is interesting to note that for both samples, $SS_{r,T}$ even at 334 K has a lower mobility than $SS_{m,T}$ at 280 K.

As seen in Table 1, the error bars for the fractions results are larger at lower temperatures, which is because the contrast of decay constants for the two components is smaller at lower temperatures. For the same reason, the error bars are smaller for 321-2k than for 211-1k. It is generally true for signal fitting that small contrasts between the components result in larger errors. This means that compared to $T_{1\rho}^{LG}$ and $T_{1\rho}^{FSLG}$ experiments, it is much easier to obtain high-quality fitting results from ^{1}H wideline (higher signal-to-noise ratio) and TD-WISE and ^{13}C–^{1}H dipolar dephasing (higher contrast of decay constants between the components). Also to be noted is that as $T_{1\rho}$ experiments involve CP, the fractions shown in Table 1 are not quantitative.

For the domains whose T_g is much raised from their intrinsic values (ca. 190 K [32,43]), an important question is the state of its dynamics between the intrinsic T_g and apparent T_g. This is difficult to assess from TD-WISE experiment as $T_{dd,mas}$ is also affected by the fast local chain rotation associated with the β relaxation. On the other hand, since this fast rotation is about three orders of magnitude faster (see next section) than the rate window of $T_{1\rho}^{FSLG}$, its effect to $T_{1\rho}^{FSLG}$ is minimal and thus a better answer to the above question can be obtained by assessing the $T_{1\rho}^{FSLG}$ data. Table 1 indicates that $T_{1\rho}^{FSLG}$ of $SS_{r,T}$ in both samples are similar and near the $T_{1\rho}^{FSLG}$ minimum at 280 K, suggesting elevated mobility at an average rate of ca. 10^5 s^{-1}. Such a mobility must be of more isotropic nature as it is on top of the motional mode associated with the β relaxation, an anisotropic chain rotation around its own contour axis at a rate of ca. 10^8 s^{-1} (see next section). At higher temperatures, the mobility of $SS_{r,T}$ becomes faster, but still considerably slower than that of $SS_{m,T}$.

It would be of interest to compare the two-component fitting results obtained from ^{1}H wideline, TD-WISE, ^{13}C–^{1}H dipolar dephasing, and $T_{1\rho}^{FSLG}$. In all the experiments, the rigid population decreases upon increasing temperature for the more phase-mixed samples. The population of $SS_{r,W}$ (by TD-WISE) is quite similar to that of $SS_{r,T}$ (by $T_{1\rho}^{FSLG}$), but not exactly the same, which may be explained by the criteria of separating the dynamical populations by $T_{dd,mas}$ and $T_{1\rho}^{FSLG}$ not being exactly the same. For example, $T_{dd,mas}$ is more dependent on sample spinning speed and the geometry (e.g. degree of isotropicity) of the segmental motion than $T_{1\rho}^{FSLG}$. The non-quantitative nature of the CP process is not a major issue here as CP would generate similar bias toward the rigid component in both cases.

3.4. SS segmental dynamics probed by ^{13}C T_1 relaxation measurements

Having seen that phase-mixing with HS substantially affects the dynamics of SS at the window of 10^5 s^{-1}, it would be of interest to see how it affects local and fast molecular dynamics (what is associated with sub-T_g relaxations), for which we conducted ^{13}C T_1 relaxation experiments. The ^{13}C T_1 values of the internal methylene (27 ppm) of PTMO in 211-1k, as measured following the Torchia method [25], are shown in Table 2. Despite the signal being a sum of both mobile and rigid fractions, the T_1 decay curves can be well fitted by single exponentials. This is similar to what has been reported in the literature [14] except that we did not observe the small (ca. 4%) slow-relaxing component which was assigned to HS/SS interface. The T_1 values are at 0.2–0.3 s for the temperature window probed, and results for other PUUs are similar [22]. This may be compared with the ^{13}C T_1 of amorphous polyethylene (PE), whose T_1 relaxation is driven by reorientation of C–H bonds in the same CH_2 structure and thus would exhibit similar relationships between segmental dynamics and relaxation times. In amorphous PE, the ^{13}C T_1 minimum occurred at 0.2–0.3 s [31], at which the segments would have a reorientation rate close to the ^{13}C Larmor frequency of 67.4 MHz. Comparing with the ^{13}C T_1 values of 0.2–0.3 s for PTMO at a similar Larmor frequency (75 MHz), we may conclude that the dynamics that drives the ^{13}C T_1 relaxation for PTMO is at ca. 10^8 s^{-1} at ambient temperature. The reason that such a fast motion does not excessively prolongs T_{dd} of ^{1}H decay for either the rigid or the mobile component must be because this motion is anisotropic. The single-exponential nature of the decays suggests that both mobile-SS and rigid-SS fractions exhibit the same fast segmental dynamics.

Such a fast dynamics should be the molecular mechanism of the β relaxation [32], which is the localized (involving rotation of a few backbone bonds) segmental rotation starting at ca. 130 K. The DMA plot of PUU samples in Fig. 6 shows a peak at ca. 130 K, regardless of PUU compositions, which presumably corresponds to the β relaxation in PTMO moiety of PUUs. Mechanical and dielectric behaviors of both neat PTMO and poly(trimethylene oxide) have been studied [32] and it was found that such relaxations occurred at ca.120 K,

Table 1
Fitting results for ^{1}H relaxation under FSLG spin lock for sample 211-1k and 321-2k. Error bars reflect the standard deviations of fitting.

Sample	T [K]	f_{fast} [%]	$T_{1\rho}^{FSLG}$(fast) [ms]	$T_{1\rho}^{FSLG}$(slow) [ms]
211-1k	280	58 ± 12	1.4 ± 0.2	3.9 ± 0.6
	300	45 ± 8	1.5 ± 0.3	5.5 ± 0.6
	322	42 ± 6	1.9 ± 0.3	8.0 ± 0.7
	334	41 ± 5	2.4 ± 0.3	10.9 ± 0.8
321-2k	280	51 ± 6	1.5 ± 0.2	5.9 ± 0.5
	300	50 ± 4	2.5 ± 0.2	13.0 ± 0.9
	334	43 ± 4	3.6 ± 0.4	24.8 ± 2.7

Table 2
^{13}C T_1 values of internal methylenes in PTMO of 211-1k. Error bars indicate standard deviations of curve fitting.

Temperature (K)	T_1 (s)
280	0.22 ± 0.03
295	0.20 ± 0.02
322	0.31 ± 0.02

which agrees with the above DMA observation in PUUs.

Due to its localized nature, the β relaxation in a PTMO domain would be little affected by its surrounding environment. The situation is similar for PE, in which low- and high-crystallinity PEs exhibit remarkably similar temperatures of γ relaxation [44,45], which has the same molecular mechanism as the β relaxation in PTMO. This is likely the reason that the rigid-SS domains also have β relaxation at full strength. On the other hand, the glass transition, a motional mode that involves the cooperation of neighboring chains and extends over a longer length scale, would be affected by factors such as phase mixing and domain size. For a given SS domain, at increasing temperature, the β relaxation will first activate, at ca. 130 K and likely regardless of its state of phase mixing. It would persist through the entire temperature range and continue to become faster in Arrhenius manner. The slower and more isotropic motional modes would activate at higher temperatures (≥210 K and dependent on the extent of phase mixing).

4. Discussions

4.1. Glass transition process in SS-rich domains

The ^{1}H wideline, TD-WISE, ^{13}C–^{1}H dipolar dephasing, $T_{1\rho}$, $T_{1\rho}^{FSLG}$, and DMA results provide multiple angles to view several aspects of the glass transition process in SS-rich domains. Data from ^{1}H wideline, ^{13}C–^{1}H dipolar dephasing, TD-WISE, and $T_{1\rho}^{FSLG}$ experiments can all be well fitted by a two-component model, all suggesting that the complex morphology of the SS-rich domains in PUU can be modeled by a two-component system. This is consistent with the dielectric results of the same samples in an earlier publication [13], in which two relaxation peaks can be seen for 211–650 and 211-1k. The glass transition that appears as large tanδ peak on DMA can be reasonably assigned to the rigid/mobile population exchange (transition from rigid to mobile fraction at increasing temperature) as observed by NMR, taking into account the shift of transition temperature between the two measurements as a result of different measuring rates. This assignment could be derived by comparing all the data for more phase-separated samples (321-2k and 211-2k) against more phase-mixed ones (211-1k and 211–650). At increasing temperature, while both groups of samples see moderately increasing mobility for both rigid and mobile fractions, the latter group shows much larger exchange of population from the rigid to the mobile fraction, which corroborates with the large tanδ values at the same temperature window. The population exchange at each step change of temperature allows us to view the broad glass transition as a sum of many transitions of sub-populations or "slices". Each "slice" would have a different T_g which is determined by the degree of phase mixing at the locale.

On the other hand, the rigid component does not appear to be completely rigid, but has a mobility that slowly increases with temperature, reaching 10^5 s^{-1} at 280 K, as observed from the $T_{1\rho}^{FSLG}$ data. This may be because the SS_r component, though do not have the freedom to undergo cooperative large-scale motions at temperature ≤ T_g, is nonetheless much above its intrinsic T_g of ca. 190 K, thus might gain some limited mobility.

For 211-1k, at each temperature probed, the $T_{1\rho}^{FSLG}$ values of the two fractions differ by a factor of 3–4. Although translating $T_{1\rho}^{FSLG}$ values to segmental motion correlation times would be dependent on the choice of correlation time model, it may be fair to state that the difference in dynamics between the two fractions is rather small, probably within an order of magnitude. This could be related to the observation that the SS_r and SS_m populations obtained at various temperatures by TD-WISE and $T_{1\rho}^{FSLG}$ are qualitatively consistent, but do not quantitatively correspond to each other, which might suggest that the transition between these two SS populations is not sharp, resulting in different criteria for defining $SS_{r,W}/SS_{m,W}$ vs. $SS_{r,T}/SS_{m,T}$. Despite these complexities, our simple model with two relaxation times seems to account for all the experimental data fairly well.

The glass transition process associated with the PTMO moiety of PUU could be compared to the dynamics in the noncrystalline (NC) region of linear polyethylene (LPE). Two factors make such a comparison meaningful. First, PTMO and PE are structurally very similar and both exhibit strong sub-T_g relaxations. Second, PTMO in PUU and noncrystalline PE are both spatially confined by rigid domains, the former by HS and the latter by crystallites. ^{2}H NMR shows that NC segments in LPE exhibit four distinct states of mobility: rigid, and rapid reorientation involving 3 bonds, 5 bonds, and ≥7 bonds [46]. From 123 K to 313 K, the NC region gradually transitions from mostly rigid to mostly 3-bond mobile, then to mostly 5-bond mobile, then to mostly ≥7-bonds mobile [46]. Therefore, the transition can be better described as exchanges between the populations with relatively constant mobility rather than a continuous increase of mobility by a single population. The transitions in SS-rich domains of PUU and noncrystalline PE both span a much wider temperature window than the transition in completely amorphous polymers such as atactic polystyrene [19], in which the transition between rigid and fast mobile states completes within a narrow temperature window.

Comparing $T_{1\rho}$ relaxations under different spin lock schemes may infer the domain sizes of the heterogeneity. The most plausible reason for $T_{1\rho}$ being mostly single-exponential while $T_{1\rho}^{FSLG}$ being bi-exponential is that the former relaxation is under the influence of spin diffusion, thus during the relaxation the signals from the various domains communicate. The spin diffusion coefficient of a relatively rigid elastomer as 211-1k can be estimated as ca. 0.4 nm^2/ms [47], It has also been reported [39] that spin diffusion under xy-SL and medium spinning speed (2–5 kHz) is slower than z-diffusion by a factor of 3–4. Therefore, the spin diffusion coefficient during xy-SL for 211-1k can be estimated as ca. 0.1 nm^2/ms. At this rate, during the course of $T_{1\rho}$ experiment, which lasts ca. 10 ms, spin diffusion would reach over a couple of nanometers. Thus we may estimate that the average size of each domain is likely smaller than 2–3 nm.

It is to be noted that by the NMR definition of rigid vs mobile SS, it is not possible to tell the difference between the motionally restricted SS that is due to spatial proximity to HS and the phase mixed SS. On the other hand, it is not necessary to make such distinction as their effects to the macroscopic properties of the materials are the same.

4.2. Mechanical behavior at high strain rates

Glass transition, unlike thermodynamic phase transitions, is rate-dependent. For example, DMA results from an earlier work on PUU elastomers indicated the shift of the SS T_g to a higher temperature as the test frequency increased [3]. More recent dielectric studies further revealed that 211-1k would become mostly glassy once the test frequency increased to ~21,000 Hz, as the frequency-dependent T_g of the phase-mixed SS approached ambient temperature, suggesting 211-1k would undergo deformation-induced glass transition upon high strain-rate (ca.10^4-10^5 s^{-1}) deformation [13].

These results reflect the time-temperature superposition principle, which predicts that when a material is under high-strain-rate deformation, it would behave similar to a deformation at low strain rate at a lower temperature. In the present report, SS_r has an average motional rate of ca. 10^5 s^{-1}; and SS_m has a dynamics that is several times faster than this. Thus, at a strain rate of 10^4 - 10^5 s^{-1}, most of the SS_r would behave rigid, and part of the SS_m whose T_g is

reached would become glassy. For phase-separated PUUs, the SS_r population is sparse and the SS_m population has lower T_g, while for phase-mixed PUUs, the SS_r population is more populous and the SS_m population has T_g's that are much closer to service temperature, leading to higher stiffness at high strain rates (higher dynamical strengthening) in the latter [3]. It has been experimentally observed [13] that PUU materials with higher phase mixing extent exhibit higher dynamical strengthening in split-Hopkinton pressure bar (SHPB) measurements (strain rate of ca. 10^3 s^{-1}), whereas deformation-induced glass transition could also be realized in phase separated PUUs upon Impulsive Stimulated Scattering (ISS) experiments (strain rate of ca. 10^8 s^{-1}). These are consistent with ssNMR observations.

5. Conclusions

^1H, TD-WISE, $^1H-^{13}C$ dipolar dephasing, and $T_{1\rho}$ experiments were conducted to discern the segmental mobility and glass transition process in select model poly(urethane urea) elastomers. At increasing temperature, the populations of SS_r and SS_m exchange, and the exchanges are more pronounced for phase-mixed samples (211–650 and 211-1k), which can be interpreted as glass transition at each step change of temperature. On the other hand, the populations of SS_r remain small and mostly unchanged in more phase separated PUUs (211-2k and 321-2k). While TD-WISE and $^1H-^{13}C$ dipolar dephasing experiments generate larger contrast of decay constants between the two populations and thus are easier to obtain high fitting quality, $T_{1\rho}^{LG}$ and $T_{1\rho}^{FSLG}$ experiments provide better assessment of mobility for both populations.

^{13}C T_1 relaxation measurements suggest a fast segmental rotation of the methylene moieties on the order of 10^8 s^{-1} at ambient temperature for both mobile- and rigid-SS. This is associated with the β relaxation observed in DMA at ca. 130 K, regardless of the PUU compositions.

These NMR measurements clearly identified several superposing relaxation modes of SS: the fast, localized segmental rotation corresponding to the β relaxation, the mostly isotropic yet restricted motion of SS_r, and the cooperative segmental motion of SS_m. Upon high-strain-rate (10^4 - 10^5 s^{-1}) deformation, most of SS_r would behave rigid and part of SS_m would become glassy, leading to dynamically induced strengthening and toughening.

Acknowledgements

This manuscript is based upon work supported by the U.S. Army Research Laboratory and the U. S. Army Research Office under grant numbers W911NF-14-1-0204 and W911NF-15-1-0534.

Appendix A. Supplementary data

Supplementary data related to this article can be found at http://dx.doi.org/10.1016/j.polymer.2016.08.015.

References

[1] C.I. Chiriac, in: H.F. Mark (Ed.), Encyclopedia of Polymer Science and Engineering, Vol. 13, John Wiley and Sons, New York, 1988, pp. 212–243.
[2] R.B. Bogoslovov, C.M. Roland, R.M. Gamache, Appl. Phys. Lett. 90 (2007) 221910.
[3] S.S. Sarva, A.J. Hsieh, Polymer 50 (2009) 3007–3015.
[4] M. Grujicic, B. Pandurangana, T. He, B.A. Cheeseman, C.-F. Yen, C.L. Randow, Mater. Sci. Eng. A 527 (2010) 7741–7751.
[5] J.T. Koberstein, A.R.S. Stein, J. Polym. Sci. Polym. Phys. Ed. 21 (1983) 1439–1472.
[6] J.T. Koberstein, L.M. Leung, Macromolecules 25 (1992) 6206–6213.
[7] C.B. Wang, S.L. Cooper, Macromolecules 16 (1983) 775–786.
[8] J.T. Koberstein, T.P. Russell, Macromolecules 19 (1986) 714–720.
[9] N.J. Clayden, C. Nijs, G. Eeckhaut, Macromolecules 31 (1998) 7820–7828.
[10] F. Yeh, B.S. Hsiao, B.B. Sauer, S. Michel, H.W. Siesler, Macromolecules 36 (2003) 1940–1954.
[11] R. Hernandez, J. Weksler, A. Padsalgikar, T. Choi, E. Angelo, J.S. Lin, L.-C. Xu, C.A. Siedlecki, J. Runt, Macromolecules 41 (2008) 9767–9776.
[12] K.E. Strawhecker, A.J. Hsieh, T.L. Chantawansri, Z.I. Kalcioglu, K.J.V. Vliet, Polymer 54 (2012) 901–908.
[13] A.J. Hsieh, T.L. Chantawansri, W. Hu, K.E. Strawhecker, D.T. Casem, J.K. Eliason, K.A. Nelson, E.M. Parsons, Polymer 55 (2014) 1883–1892.
[14] M. Ishida, K. Yoshinaga, F. Horii, Macromolecules 29 (1996) 8824–8829.
[15] J.A. Kornfield, H.W. Spiess, H. Nefzger, H. Hayen, C.D. Eisenbach, Macromolecules 24 (1991) 4787–4795.
[16] H.-J. Tao, D.M. Rice, W.J. MacKnight, S.L. Hsu, Macromolecules 28 (1995) 4036–4038.
[17] D.T. Okamoto, S.L. Cooper, T.W. Root, Macromolecules 25 (1992) 1068–1073.
[18] J.D. Menczel, L. Judovits, R.B. Prime, H.E. Bair, M. Reading, S. Swier, Thermal Analysis of Polymers, Fundamentals and Applications, first ed., Wiley, John & Sons, Incorporated, 2009.
[19] G.R. Strobl, The Physics of Polymers, Springer, 1996.
[20] R.A. Assink, Macromolecules 11 (1978) 1233–1237.
[21] R.A. Assink, G.L. Wilkes, J. Appl. Polym. Sci. 26 (1981) 3689–3698.
[22] W. Hu, A.J. Hsieh, Polymer 54 (2013) 6218–6225.
[23] C. Hedesiu, D.E. Demco, R. Kleppinger, A.A. Buda, B. Blumich, K. Remerie, V.M. Litvinov, Polymer 48 (2007) 763–777.
[24] K. Schmidt-Rohr, J. Clauss, H.W. Spiess, Macromolecules 25 (1992) 3273–3277.
[25] D.A. Torchia, J. Magn. Res. 30 (1978) 613–616.
[26] E.W. Hansen, P.E. Kristiansen, B. Pedersen, J. Phys. Chem. B 102 (1998) 5444–5450.
[27] C. Hertlein, K. Saalwächter, G. Strobl, Polymer 47 (2006) 7216–7221.
[28] R. Zhang, S. Yu, S. Chen, Q. Wu, T. Chen, P. Sun, B. Li, D. Ding, J. Phys. Chem. B 118 (2014) 1126–1137.
[29] L.B. Alemany, D.M. Grant, T.D. Alger, R.J. Pugmire, J. Am. Chem. Soc. 105 (1983) 6697–6704.
[30] Y. Huang, D.F.R. Gilson, I.S. Butler, F. Morin, J. Phys. Chem. 95 (1991) 2151–2156.
[31] Q. Chen, T. Yamada, H. Kurosu, I. Ando, T. Shiono, Y. Doi, J. Polym. Sci. Part B Polym. Phys. 30 (1992) 591–601.
[32] N.G. McCrum, B.E. Read, G. Williams, Anelastic and Dielectric Effects in Polymeric Solids, Dover, 1967.
[33] A.J. Vega, R.W. Vaughan, J. Chem. Phys. 68 (1978) 1958–1966.
[34] P. Mansfield, J. Orchard, D.C. Stalker, K.H.B. Richards, Phys. Rev. B7 (1973) 90–105.
[35] W.-K. Rhim, D.D. Elleman, R.W. Vaughan, J. Chem. Phys. 59 (1973) 3740–3749.
[36] D.L. VanderHart, C.R. Snyder, Macromolecules 36 (2003) 4813–4826.
[37] D.L. VanderHart, G.B. McFadden, Solid State Nucl. Magn. Reson 7 (1996) 45–66.
[38] M. Lee, W.I. Goldburg, Phys. Rev. A 140 (1965) 1261.
[39] Q. Chen, K. Schmidt-Rohr, Solid State Nucl. Magn. Reson 29 (2006) 142–152.
[40] B.-J. Van Rossum, H. Forster, H.J.M. De Groot, J. Magn. Res. 124 (1997) 516–519.
[41] R. Fu, J. Hu, T.A. Cross, J. Magn. Res. 168 (2004) 8–17.
[42] R. Fu, C. Tian, T.A. Cross, J. Magn. Res. 154 (2002) 130–135.
[43] J. Brandrup, E.H. Immergut, E.A. Grulke, Polymer Handbook, 1999.
[44] R.H. Boyd, Macromolecules 17 (1984) 903–911.
[45] R.H. Boyd, Polymer 26 (1985) 323–347.
[46] D. Hentschel, H. Sillescu, H.W. Spiess, Polymer 25 (1984) 1078–1086.
[47] F. Mellinger, M. Wilhelm, H.W. Spiess, Macromolecules 32 (1999) 4686–4691.